ESPOO 2003 VTT PUBLICATIONS 513

Seppo Uosukainen

Turbulences as sound sources

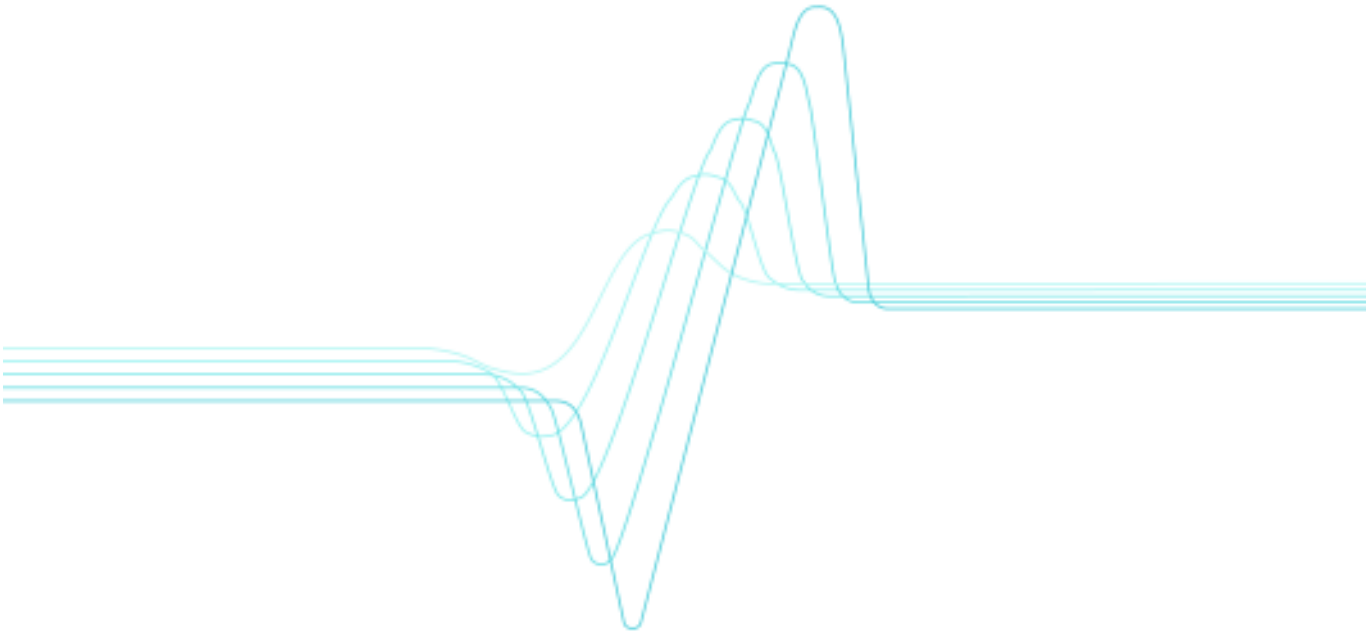

VTT PUBLICATIONS 513

Turbulences as sound sources

Seppo Uosukainen

VTT Building and Transport

ISBN 951–38–6257–7 (soft back ed.)
ISSN 1235–0621 (soft back ed.)

ISBN 951–38–6258–5 (URL: http://www.vtt.fi/inf/pdf/)
ISSN 1455–0849 (URL: http://www.vtt.fi/inf/pdf/)

JULKAISIJA – UTGIVARE – PUBLISHER

VTT, Vuorimiehentie 5, PL 2000, 02044 VTT
puh. vaihde (09) 4561, faksi (09) 456 4374

VTT, Bergsmansvägen 5, PB 2000, 02044 VTT
tel. växel (09) 4561, fax (09) 456 4374

VTT Technical Research Centre of Finland, Vuorimiehentie 5, P.O.Box 2000, FIN–02044 VTT, Finland
phone internat. + 358 9 4561, fax + 358 9 456 4374

VTT Rakennus- ja yhdyskuntatekniikka, Lämpömiehenkuja 3, PL 1804, 02044 VTT
puh. vaihde (09) 4561, faksi (09) 456 4709

VTT Bygg och transport, Värmemansgränden 3, PB 1804, 02044 VTT
tel. växel (09) 4561, fax (09) 456 4709

VTT Building and Transport, Lämpömiehenkuja 3, P.O.Box 1804, FIN–02044 VTT, Finland
phone internat. + 358 9 4561, fax + 358 9 456 4709

Technical editing Marja Kettunen

Otamedia Oy, Espoo 2003

Uosukainen, Seppo. Turbulences as sound sources. Espoo 2003. VTT Publications 513. 42 p.

Keywords noise, jet noise, turbulence, turbulent flow, vortex flow, air jets, Reynolds' stress, boundary layers

Abstract

The aerodynamic sound source of a turbulent flow with a high Reynolds' number is composed of two types of Reynolds' stress components containing turbulent vortices as elements: perturbation–perturbation solenoidal velocity interaction (self-noise) and perturbation–static velocity interaction (shear-noise). The vortices act as quadrupole sources. Near a scattering surface, a high turbulent velocity imparts high fluctuating forces to it and couples to sound causing the scattered sound to be even stronger than the original one. The high-Reynolds'-number subsonic cold-air jet structure, beginning from a nozzle and developing gradually to solenoidal and turbulent, consists of a mixing region, a transition region, and a fully developed region. Most of the sound power originates from the mixing region. The spectrum of the jet noise is of broadband character. The typical radiation pattern of a quadrupole distribution is totally masked by convectional effects of the jet flow, which tend to enhance the sound greatly in the flow direction. The sound propagating in the jet flow direction will be refracted sidewards, causing a cone centered on the downstream jet axis wherein the far field sound is greatly reduced (zone of silence), and tending to decline the lobe of the radiation pattern. When a flow attacks a plate parallel to its surface at Reynolds' numbers high enough, there begins to form unsteady vortices, forming a turbulent boundary layer. The wavenumber spectrum in the turbulent boundary layer has two maxima: the convective peak at a high subsonic wavenumber and the sonic peak at the acoustic wavenumber. The sonic and supersonic spectral components at the surface generate active propagating sound, most of the acoustic energy propagating at grazing incidence downstream. Downstream propagating sound due to the wavenumber components near the sonic peak refracts towards the surface, and upstream propagating sound refracts outwards from the surface, enhancing the sonic peak in the downstream radiation and possibly eliminating it in the upstream radiation. The convective peak at the surface leads to the hydrodynamic coincidence, causing sound transmission and radiation at frequencies below the hydrodynamic coincidence frequency.

Preface

The work described in this report has been carried out at VTT Building and Transport, Structures and Building Services, Technical Building Services, Acoustics Team. The results have been obtained through FACE project (Friendly Aircraft Cabin Environment), an ongoing EU project which started in fifth Framework Programme (GROWTH) in 2002. The work done is connected to Work Package 5 (Environmental Comfort Procedures), ANVC part (Active Noise and Vibration Control) in Work Task 5.1 (Scientific Approaches with Respect to Noise and Vibrations) in FACE project. The aim of this report is to describe the noise source mechanisms and the properties of the noise in subsonic cold-air jets and turbulent boundary layers. Jet noise, turbulent boundary noise, and buzz-saw noise are remarkable noise components in the cabins of jet-powered aircraft.

Mrs. Leila Uosukainen has revised the language of this work.

Espoo, November 2003

Seppo Uosukainen
e-mail: Seppo.Uosukainen@vtt.fi

Contents

List of symbols

c	local speed of sound in constant enthropy
c_0	first order value of c
c_f	skin-friction coefficient
D	diameter of nozzle
$\overline{\overline{E}}$	rate-of-strain dyadic
$\overline{\overline{E}}_0$	static component of rate-of-strain dyadic
$\overline{\overline{E}}_{01}$	the part of $\overline{\overline{E}}_0$ composed of irrotational velocity
$\overline{\overline{E}}_{02}$	the part of $\overline{\overline{E}}_0$ composed of solenoidal velocity
$\overline{\overline{e}}$	perturbation component of rate-of-strain dyadic
$\overline{\overline{e}}_1$	the part of $\overline{\overline{e}}$ composed of irrotational velocity
$\overline{\overline{e}}_2$	the part of $\overline{\overline{e}}$ composed of solenoidal velocity
$\vec{e}_n$	unit normal vector
$\vec{\mathrm{e}}_x$	unit vector in x-direction
$\vec{F}$	strength of force source distribution (dipole distribution + gravitation)
f	frequency
f_{cr}	critical frequency (coincidence frequency)
f_{crM}	hydrodynamic coincidence frequency

f_s planar perturbation force source density (perturbation force per unit area, planar dipole distribution)

G_{pp} autospectrum

$\overline{\overline{\mathrm{I}}}$ identic dyadic

K constant in Equation (33)

$\vec{k}$ wavenumber vector

k_1, k_2 wavenumber components in x-direction and in orthogonal direction

L typical dimension

l correlation length

M jet Mach number

M_0 free-stream Mach number

M_c convection Mach number

P pressure

P_0 static pressure

P' power per unit length

p perturbation pressure (sound pressure)

q' strength of mass source distribution (monopole distribution, volume velocity distribution)

q_s planar mass source density (planar monopole density, planar volume velocity)

Re	Reynolds' number
R_{pp}	spatial autocorrelation function of pressure
r	distance from nozzle
r_0	radial distance from jet axis
S	surface
S	Strouhal number
S_0	constant enthropy
$\mathrm{T}_{(\mathrm{subscript})}$	transpose
$\overline{\overline{T}}$	momentum source distribution (quadrupole distribution)
$\overline{\overline{T}}_R$	aerodynamic sound source part of Reynolds' stress
$\overline{\overline{T}}_{Uu}$	shear-noise part of $\overline{\overline{T}}_R$
$\overline{\overline{T}}_{uu}$	self-noise part of $\overline{\overline{T}}_R$
t	time
$\vec{U}$	particle velocity
$\vec{U}_0$	static velocity
$\vec{U}_{01}$	irrotational part of static velocity (free-stream velocity)
$\vec{U}_{02}$	solenoidal part of static velocity
U_c	eddy convection velocity
U_j	jet velocity in nozzle

$\vec{u}$	perturbation velocity
$\vec{u}_1$	irrotational part of perturbation velocity
$\vec{u}_2$	solenoidal part of perturbation velocity
u_τ	friction velocity
V	volume
x, y	Cartesian coordinates
δ	boundary layer thickness
δ^*	boundary layer displacement thickness
$\delta(x)$	Dirac delta function
Δp	discontinuity in perturbation pressure
$\Delta\vec{u}$	discontinuity in perturbation velocity
$\Delta\rho'$	discontinuity in perturbation density
$\Delta\overline{\overline{\sigma'}}$	discontinuity in $\overline{\overline{\sigma'}}$
$\varepsilon(x)$	step function
λ	wavelength
ν	kinematic viscosity
θ	angle between observation direction and jet axis
θ_c	limiting angle of zone of silence

ξ_1, ξ_2	spatial variables of R_{pp} in flow direction and in direction orthogonal to flow
μ	coefficient of viscosity
μ_v	expansion coefficient of viscosity
ρ	density of fluid
ρ_0	static density
ρ'	perturbation density
$\bar{\bar{\sigma}}_\mu$	viscous part of stress dyadic
$\bar{\bar{\sigma}}_0$	static part of $\bar{\bar{\sigma}}_\mu$
$\bar{\bar{\sigma}}'$	perturbation part of $\bar{\bar{\sigma}}_\mu$
τ	correlation time
τ_ω	shear stress
Φ	frequency dependent part of R_{pp} and G_{pp}
ω	angular frequency
$\hat{}$	Fourier transform

1. Introduction

The aerodynamic sound sources of a turbulent flow are defined. Defining true aerodynamic sound sources is not very obvious. Indeed, the various approaches in literature, e.g. those of Lighthill, Phillips, and Lilley, define the source and field parts differently [1]. Actually, e.g. in Lighthill's turbulence stress tensor, presenting the aerodynamic sound source, the terms presenting the viscous and thermal losses in The Navier-Stokes' equation are also included. In this paper those terms are not regarded as aerodynamic sound source terms (rather acoustic sinks), and it is further assumed that the aerodynamic sound source quantities can be (approximately) separated from the acoustic field variables which give a proper condition for defining the aerodynamic sound sources. This leads to a solution where the aerodynamic sources are composed of the Reynolds' stresses, all the terms containing irrotational perturbation velocity and perturbation density excluded.

Typically, the aerodynamic sound sources are treated and their most influencing components are defined using integrals of source densities utilizing proper Green's functions, see, e.g., [1] and [2]. In this paper the source quantities are defined using basic non-linear equations of fluid (the equation of continuity and the Navier-Stokes' equation), without any source volume integrations. This gives a better insight into the physics of the source properties.

The effect of scattering surfaces to the aerodynamic sound is treated utilizing Huygens' principle of secondary sources. The secondary sources are defined using the basic non-linear equations of fluid as well.

As examples of aerodynamic sound sources, the noise of a high-Reynolds'-number subsonic cold-air jet and the noise of a turbulent boundary layer are examined. These examinations are mainly based on literature, on References [1], [2], [3], [4], and [5].

Some of the references mentioned are not original; in this case generally well-known subjects are referred to.

2. Basic equations

The non-linearized equation of continuity is, see, e.g., [1]

$$\frac{\partial \rho}{\partial t} + \nabla \cdot \left(\rho \vec{U} \right) = \rho q' , \tag{1}$$

where ρ is the density of the fluid, $\vec{U}$ is the particle velocity, t is time, and q' is the strength of the mass source distribution (monopole distribution, volume velocity distribution). The non-linearized Navier-Stokes' equation can be written in the following alternative ways (the connection between them being the equation of continuity above) [1]

$$\rho \frac{\partial \vec{U}}{\partial t} + \rho \vec{U} \cdot \nabla \vec{U} = -\nabla P + \nabla \cdot \overline{\overline{\sigma}}_{\mu} + \vec{F} - \nabla \cdot \overline{\overline{T}} \tag{2}$$

$$\frac{\partial \left(\rho \vec{U} \right)}{\partial t} + \nabla \cdot \left(\rho \vec{U} \vec{U} \right) = -\nabla P + \nabla \cdot \overline{\overline{\sigma}}_{\mu} + \rho q' \vec{U} + \vec{F} - \nabla \cdot \overline{\overline{T}} , \tag{3}$$

where P is the pressure, $\vec{F}$ is the strength of the force source distribution (dipole distribution + gravitation), $\overline{\overline{T}}$ is the momentum source distribution (quadrupole distribution), and $\overline{\overline{\sigma}}_{\mu}$ is the viscous part of the stress dyadic

$$\overline{\overline{\sigma}}_{\mu} = \left(\mu_{\nu} \overline{\overline{E}} : \overline{\overline{I}} \right) \overline{\overline{I}} + 2\mu \left[\overline{\overline{E}} - \tfrac{1}{3} \left(\overline{\overline{E}} : \overline{\overline{I}} \right) \overline{\overline{I}} \right], \tag{4}$$

where μ is the coefficient of viscosity, μ_{ν} is the expansion coefficient of viscosity, $\overline{\overline{I}}$ is the identic dyadic ($\overline{\overline{I}} \cdot \vec{a} = \vec{a}$, where $\vec{a}$ is an arbitrary vector), and $\overline{\overline{E}}$ is the rate-of-strain dyadic

$$\overline{\overline{E}} = \tfrac{1}{2} \left[\nabla \vec{U} + \left(\nabla \vec{U} \right)_{\mathrm{T}} \right], \tag{5}$$

where subscript "T" denotes the transpose of a dyadic.

The second version of the Navier-Stokes' equation can be presented as

$$\frac{\partial\left(\rho\vec{U}\right)}{\partial t}+c^2\nabla\rho-\nabla\cdot\left[\overline{\overline{\sigma}}_{\mu}-\left(P-c^2\rho\right)\overline{\overline{\mathrm{I}}}\right]+\rho\nabla c^2 \\ =-\nabla\cdot\left(\overline{\overline{T}}+\rho\vec{U}\vec{U}\right)+\rho q'\vec{U}+\vec{F}\,, \tag{6}$$

where c is the local speed of sound in constant enthropy, defined by

$$c^2=\left(\frac{\partial P}{\partial\rho}\right)_{S_0}\,, \tag{7}$$

where S_0 is the constant enthropy.

3. Reynolds' stresses

The left-hand side of the last version of the Navier-Stokes' equation contains now terms associated only to the acoustic field quantities. Its third term is attached to the viscous and thermal losses (assuming there are no thermal sources), and its fourth term is attached to the inhomogenity of the fluid. The right-hand side contains source terms, and Reynolds' stress $\rho\vec{U}\vec{U}$ behaves like quadrupole source distribution $\overline{\overline{T}}$. Indeed, the Reynolds' stresses contain quadrupole source characteristics, but part of the stresses belongs to the acoustic field quantities. The next task is to find the true aerodynamic sound source part $\overline{\overline{T}}_R$ of the Reynolds' stress. It is not very obvious what the true aerodynamic sound source part of the Reynolds' stress is. Indeed, the various approaches in literature, e.g. those of Lighthill, Phillips, and Lilley, define the source and field parts differently [1]. Actually, e.g. in Lighthill's turbulence stress tensor, presenting the aerodynamic sound source, the terms presenting the viscous and thermal losses in The Navier-Stokes' equation are also included. In this paper those terms are not regarded as aerodynamic sound source terms (rather acoustic sinks), and it is further assumed that the aerodynamic sound source quantities can be (approximately) separated from the acoustic field variables which give a proper condition for defining the true aerodynamic sound source part of the Reynolds' stress.

The divergence of the Reynolds' stress is

$$\begin{aligned}\nabla\cdot\left(\rho\vec{U}\vec{U}\right) &= (\nabla\rho)\cdot\vec{U}\vec{U}+\rho\nabla\cdot\left(\vec{U}\vec{U}\right)\\ &= (\nabla\rho)\cdot\vec{U}\vec{U}+\rho\left[\left(\nabla\cdot\vec{U}\right)\vec{U}+\vec{U}\cdot\left(\nabla\vec{U}\right)\right].\end{aligned} \tag{8}$$

Because

$$\nabla\vec{U}=\tfrac{1}{2}\left[\nabla\vec{U}+\left(\nabla\vec{U}\right)_{\mathrm{T}}\right]+\tfrac{1}{2}\left[\nabla\vec{U}-\left(\nabla\vec{U}\right)_{\mathrm{T}}\right]=\overline{\overline{E}}-\tfrac{1}{2}\left(\nabla\times\vec{U}\right)\times\bar{\bar{\mathrm{I}}} \tag{9}$$

$$\begin{aligned}\vec{U}\cdot\left(\nabla\vec{U}\right) &= \vec{U}\cdot\left(\nabla\vec{U}\right)+\vec{U}\times\left(\nabla\times\vec{U}\right)+\left(\nabla\times\vec{U}\right)\times\vec{U}\\ &= \tfrac{1}{2}\nabla\left(\vec{U}\cdot\vec{U}\right)+\left(\nabla\times\vec{U}\right)\times\vec{U},\end{aligned} \tag{10}$$

(where in the second equation it has been utilized that $\vec{a}\times\vec{b}=-\vec{b}\times\vec{a}$ for any vectors,) the divergence of the Reynolds' stress can be given in the following alternative formulae (in the first equation it will be utilized that $\vec{a}\times\overline{\overline{\mathrm{I}}}$ is antisymmetric for any vector $\vec{a}$)

$$\begin{aligned}\nabla\cdot\left(\rho\vec{U}\vec{U}\right)&=\left(\nabla\rho\right)\cdot\vec{U}\vec{U}+\rho\left[\left(\nabla\cdot\vec{U}\right)\vec{U}+\vec{U}\cdot\overline{\overline{E}}+\tfrac{1}{2}\left(\nabla\times\vec{U}\right)\times\vec{U}\right]\\&=\left(\nabla\rho\right)\cdot\vec{U}\vec{U}+\rho\left[\left(\nabla\cdot\vec{U}\right)\vec{U}+\tfrac{1}{2}\nabla\left(\vec{U}\cdot\vec{U}\right)+\left(\nabla\times\vec{U}\right)\times\vec{U}\right].\end{aligned}\qquad(11)$$

The first expression is better because with it, finding the true aerodynamic sound source part of the Reynolds' stress is much easier. Therefore, the first expression is used below.

Suppose the velocity field can be divided into static component $\vec{U}_0$ and perturbation component $\vec{u}$ so that the static component only depends on spatial coordinates and the perturbation components also depend on time. Suppose further that the static and perturbation velocity contain irrotational parts $\vec{U}_{01}$ and $\vec{u}_1$ and solenoidal parts $\vec{U}_{02}$ and $\vec{u}_2$ so that

$$\begin{aligned}\vec{U}&=\vec{U}_0+\vec{u}\\\vec{U}_0&=\vec{U}_{01}+\vec{U}_{02}\\\vec{u}&=\vec{u}_1+\vec{u}_2\\\nabla\times\vec{U}_{01}&=0\\\nabla\cdot\vec{U}_{02}&=0\\\nabla\times\vec{u}_1&=0\\\nabla\cdot\vec{u}_2&=0.\end{aligned}\qquad(12)$$

The rate-of-strain dyadic $\overline{\overline{E}}$ has now static component $\overline{\overline{E}}_0$ and perturbation component $\overline{\overline{e}}$ which can further be divided into components $\overline{\overline{E}}_{01}$, $\overline{\overline{E}}_{02}$, $\overline{\overline{e}}_1$ and $\overline{\overline{e}}_2$ associated with the corresponding velocity gradients

$$
\begin{aligned}
\overline{\overline{E}} &= \overline{\overline{E}}_0 + \overline{\overline{e}} \\
\overline{\overline{E}}_0 &= \overline{\overline{E}}_{01} + \overline{\overline{E}}_{02} \\
\overline{\overline{e}} &= \overline{\overline{e}}_1 + \overline{\overline{e}}_2 \\
\overline{\overline{E}}_{01} &= \tfrac{1}{2}\left[\nabla\vec{U}_{01} + \left(\nabla\vec{U}_{01}\right)_{\mathrm{T}}\right] \\
\overline{\overline{E}}_{02} &= \tfrac{1}{2}\left[\nabla\vec{U}_{02} + \left(\nabla\vec{U}_{02}\right)_{\mathrm{T}}\right] \\
\overline{\overline{e}}_1 &= \tfrac{1}{2}\left[\nabla\vec{u}_1 + \left(\nabla\vec{u}_1\right)_{\mathrm{T}}\right] \\
\overline{\overline{e}}_2 &= \tfrac{1}{2}\left[\nabla\vec{u}_2 + \left(\nabla\vec{u}_2\right)_{\mathrm{T}}\right].
\end{aligned}
\tag{13}
$$

Suppose further that the density ρ can be similarly divided into static component ρ_0 and perturbation component ρ' so that the static component only depends on spatial coordinates and the perturbation components also depend on time

$$
\rho = \rho_0 + \rho'. \tag{14}
$$

The divergence of the Reynolds' stress can now be written as

$$
\begin{aligned}
&\nabla\cdot\left(\rho\vec{U}\vec{U}\right) \\
&= (\nabla\rho)\cdot\vec{U}\vec{U} + \rho\left\{\left[\nabla\cdot\left(\vec{U}_{01} + \vec{u}_1\right)\right]\vec{U} + \vec{U}\cdot\overline{\overline{E}} + \tfrac{1}{2}\left[\nabla\times\left(\vec{U}_{02} + \vec{u}_2\right)\right]\times\vec{U}\right\}.
\end{aligned}
\tag{15}
$$

Far from the sound sources the particle velocity of the sound field is composed primarily of the irrotational component $\vec{u}_1$ of the perturbation velocity (except near boundaries). The perturbation component ρ' of the density is attached to the sound field. It is assumed that the aerodynamic sound source part of the Reynolds' stress can be separated from the acoustic field variables. With this assumption, all the terms containing irrotational perturbation velocity and perturbation density have to be excluded from the true aerodynamic sound source part of the Reynolds' stress. Also purely static terms have to be excluded from the acoustic source. By doing this exclusion, the divergence of the aerodynamic sound source part of the Reynolds' stress can be seen to be

$$
\begin{aligned}
\nabla\cdot\left(\overline{\overline{T}}_R\right) &= \nabla\rho_0\cdot\left(\vec{U}_0\vec{u}_2+\vec{u}_2\vec{U}_0+\vec{u}_2\vec{u}_2\right)\\
&\quad+\rho_0\Big[\left(\nabla\cdot\vec{U}_{01}\right)\vec{u}_2+\left(\vec{U}_0+\vec{u}_2\right)\cdot\overline{\overline{e}}_2+\vec{u}_2\cdot\overline{\overline{E}}_0\\
&\quad+\tfrac{1}{2}\left(\nabla\times\vec{u}_2\right)\times\left(\vec{U}_0+\vec{u}_2\right)+\tfrac{1}{2}\left(\nabla\times\vec{U}_{02}\right)\times\vec{u}_2\Big]\\
&=\nabla\rho_0\cdot\left(\vec{U}_0\vec{u}_2+\vec{u}_2\vec{U}_0+\vec{u}_2\vec{u}_2\right)+\rho_0\Big\{\left(\nabla\cdot\vec{U}_{01}\right)\vec{u}_2\\
&\quad+\left(\vec{U}_0+\vec{u}_2\right)\cdot\left[\overline{\overline{e}}_2-\tfrac{1}{2}\left(\nabla\times\vec{u}_2\right)\times\overline{\overline{\mathrm{I}}}\right]+\vec{u}_2\cdot\left[\overline{\overline{E}}_0-\tfrac{1}{2}\left(\nabla\times\vec{U}_{02}\right)\times\overline{\overline{\mathrm{I}}}\right]\Big\}.
\end{aligned}
\tag{16}
$$

The non-source part of the divergence of the Reynolds' stress $\nabla\cdot\left(\overline{\overline{T}}-\overline{\overline{T}}_R\right)$ should thus be interpreted as field terms in the Navier-Stokes' equation.

It can be seen that the aerodynamic sound source is mainly formed of the gradient, divergence and curl of the static velocity component $\vec{U}_0$, and the gradient and curl of the solenoidal perturbation velocity component $\vec{u}_2$. Terms originating from the gradient of the static density also appear in the aerodynamic sound source presentation. If the static density is not a function of spatial coordinates, these terms disappear.

The aerodynamic sound source part of the Reynolds' stress can be further divided into two components so that

$$
\nabla\cdot\left(\overline{\overline{T}}_R\right)=\nabla\cdot\left(\overline{\overline{T}}_{uu}+\overline{\overline{T}}_{Uu}\right),
\tag{17}
$$

where

$$
\begin{aligned}
\nabla\cdot\left(\overline{\overline{T}}_{uu}\right) &= \nabla\rho_0\cdot\vec{u}_2\vec{u}_2+\rho_0\left[\vec{u}_2\cdot\overline{\overline{e}}_2+\tfrac{1}{2}\left(\nabla\times\vec{u}_2\right)\times\vec{u}_2\right]\\
&=\nabla\rho_0\cdot\vec{u}_2\vec{u}_2+\rho_0\left\{\vec{u}_2\cdot\left[\overline{\overline{e}}_2-\tfrac{1}{2}\left(\nabla\times\vec{u}_2\right)\times\overline{\overline{\mathrm{I}}}\right]\right\}
\end{aligned}
\tag{18}
$$

and

$$\nabla\cdot\left(\overline{\overline{T}}_{Uu}\right)=\nabla\rho_0\cdot\left(\vec{U}_0\vec{u}_2+\vec{u}_2\vec{U}_0\right)$$
$$+\rho_0\left[\left(\nabla\cdot\vec{U}_{01}\right)\vec{u}_2+\vec{U}_0\cdot\overline{\overline{e}}_2+\vec{u}_2\cdot\overline{\overline{E}}_0+\tfrac{1}{2}\left(\nabla\times\vec{u}_2\right)\times\vec{U}_0+\tfrac{1}{2}\left(\nabla\times\vec{U}_{02}\right)\times\vec{u}_2\right] \quad (19)$$
$$=\nabla\rho_0\cdot\left(\vec{U}_0\vec{u}_2+\vec{u}_2\vec{U}_0\right)$$
$$+\rho_0\left\{\left(\nabla\cdot\vec{U}_{01}\right)\vec{u}_2+\vec{U}_0\cdot\left[\overline{\overline{e}}_2-\tfrac{1}{2}\left(\nabla\times\vec{u}_2\right)\times\overline{\overline{\mathrm{I}}}\right]+\vec{u}_2\cdot\left[\overline{\overline{E}}_0-\tfrac{1}{2}\left(\nabla\times\vec{U}_{02}\right)\times\overline{\overline{\mathrm{I}}}\right]\right\}.$$

The first part generates so called self-noise and the second part shear-noise. The self-noise is associated with perturbation–perturbation velocity interaction while the shear-noise is associated with perturbation–static velocity interaction [1]. The perturbation–static velocity interaction can be seen as a phenomenon where the perturbation vorticity is carried along with the static flow. When the static velocity (and especially its gradient, divergence, and curl) is much higher than the perturbation velocity, the perturbation–perturbation velocity interaction is of second order and it can be omitted, in which case

$$\overline{\overline{T}}_R\approx\overline{\overline{T}}_{Uu}. \quad (20)$$

It can be seen that in this case, both the static velocity and the solenoidal part of the perturbation velocity are needed to obtain sound radiation.

Because the Reynolds' stress behaves like a momentum source distribution in the Navier-Stokes' equation (momentum balance equation), its physical significance is that it gives momentum to the acoustic field from the static flow. With the help of this increase in momentum, it is possible that the solenoidal part of the perturbation velocity, being the actual cause of the sound, can increase in proper configurations.

Using dimensional analysis in the Navier-Stokes' equation, one can conclude that the Reynolds' stress compared to the viscous stress is of the order

$$Re=\frac{\rho UL}{\mu}, \quad (21)$$

where L is a typical dimension of the aerodynamic sound source region (vortex size) of the Reynolds' stress. The non-dimensional parameter *Re* is called the

Reynolds' number. When the Reynolds' number is much higher than one, the effect of the Reynolds' stress dominates the effect of the viscous stress. Assuming that the Prandtl number, describing the ratio of the viscous and thermal losses, is near one (which is the case of air), the effect of thermal losses is also much lower than that of the Reynolds' stress in the case of a high Reynolds' number. Because the viscous and thermal losses in the Navier-Stokes' equation describe the decrease of momentum due to losses, the high Reynolds' number assures that the flow gives more momentum to the acoustic field than the internal losses decrease it. Therefore, it can be concluded that the Reynolds' stress can be a remarkable source of sound only in the case of a high Reynolds' number.

With the Reynolds' numbers higher than about 1200, the vortices appear turbulent. Outside turbulent regions of flow, the efficiency of the aerodynamic sound source part of the Reynolds' stress is negligible. [1]

4. Equivalent Huygens' sources

As well as the velocity and density, the pressure and the viscous part of the stress dyadic can be divided into static components (subscript "0") and perturbation components

$$\begin{aligned} P &= P_0 + p \\ \overline{\overline{\sigma}}_\mu &= \overline{\overline{\sigma}}_0 + \overline{\overline{\sigma}}'. \end{aligned} \tag{22}$$

In the next, the monopole and dipole sources are supposed to be planar perturbation sources (the gravitation is omitted), situating at plane $x = 0$, i.e.,

$$\begin{aligned} q' &= q_s \delta(x) \\ \vec{F} &= \vec{f}_s \delta(x), \end{aligned} \tag{23}$$

where $\delta(x)$ is a Dirac delta function. Quantities q_s and f_s are thus planar source densities (volume velocity and force per unit area). Inserting these to the equation of continuity and to the (first version of the) Navier-Stokes' equation shows that the Dirac delta function can be obtained only from the discontinuity of the divergence and gradient terms in the equations. By inserting the expression

$$\nabla \cdot \left(\rho \vec{U}\right) = (\nabla \rho) \cdot \vec{U} + \rho \nabla \cdot \vec{U} \tag{24}$$

to the equation of continuity, one can notice that the density must contain the term $\Delta\rho'\varepsilon(x)$ and the velocity must contain the term $\Delta\vec{u}\varepsilon(x)$, where $\varepsilon(x)$ is a step function. Taking the gradient of the density and the divergence of the velocity yields Dirac delta functions from the step functions. Integrating the continuity equation over a small path across $x = 0$, the planar monopole distribution can be seen to be

$$q_s = \left(\Delta\vec{u} + \frac{\Delta\rho'}{\rho} \vec{U} \right) \cdot \vec{e}_x, \tag{25}$$

where $\vec{e}_x$ is a unit vector in the x-direction.

Like in the (first version of the) Navier-Stokes' equation, one can notice that the pressure must contain the term $\Delta p\varepsilon(x)$, the velocity must contain the term $\Delta\vec{u}\varepsilon(x)$, and the viscous part of the stress dyadic must contain the term $\Delta\sigma'\varepsilon(x)$. Before inserting these into the equation, the Navier-Stokes' equation is modified a little. Using Equation (10), one can deduce that

$$\vec{U}\cdot\nabla\vec{U} = -\vec{U}\times\left[\nabla\times\left(\vec{U}_0+\vec{u}\right)\right]+\tfrac{1}{2}\nabla\left(\vec{U}_0\cdot\vec{U}_0\right)+\tfrac{1}{2}\nabla\left(\vec{u}\cdot\vec{u}\right)+\nabla\left(\vec{U}_0\cdot\vec{u}\right). \quad (26)$$

Inserting this and the discontinuous terms into the Navier-Stokes' equation and integrating it over a small path across $x = 0$, the planar dipole distribution can be seen to be

$$\vec{f}_s = \left[\Delta p+\rho\left(\vec{U}_0\cdot\Delta\vec{u}+\tfrac{1}{2}\Delta\vec{u}\cdot\Delta\vec{u}\right)\right]\vec{e}_x+\rho\vec{U}\times\left(\Delta\vec{u}\times\vec{e}_x\right)-\vec{e}_x\cdot\Delta\overline{\overline{\sigma'}}. \quad (27)$$

Thus, the planar source distributions can be obtained from the field discontinuities using Equations (25) and (27).

In the Huygens' principle, the effect of a radiating, absorbing, or scattering (reflecting and/or diffracting) region V to the other part of the space can be taken into account by equivalent Huygens' sources distributed on any closed surface enclosing V, see, e.g., [6]. The equivalent sources have no effect inside the closed surface. So the equivalent surface source distributions at surface S enclosing region V, see Figure 1, are similar to those presented above, the discontinuities of the fields replaced by the actual field values at the surface. Thus, the equivalent Huygens' sources at the surface are obtained from the fields at the surface, analogously with Equations (25) and (27), from equations

$$q_s = \left(\vec{u}+\frac{\rho'}{\rho}\vec{U}\right)\cdot\vec{e}_n \quad (28)$$

$$\vec{f}_s = \left[p+\rho\left(\vec{U}_0\cdot\vec{u}+\tfrac{1}{2}\vec{u}\cdot\vec{u}\right)\right]\vec{e}_n+\rho\vec{U}\times\left(\vec{u}\times\vec{e}_n\right)-\vec{e}_n\cdot\overline{\overline{\sigma'}}, \quad (29)$$

where $\vec{e}_n$ is a unit normal vector outwards from the surface, see Figure 1. Supposing the perturbation fields are much smaller than the static ones (the velocity does not have to obey this), the first order terms of the Huygens' sources can only be used. Supposing the viscous losses are small (in which case the

effect of the viscous part of the stress dyadic and the term originating from the vorticity of the perturbation velocity can be omitted), and supposing the thermal losses are small (this yielding to $\rho' = p/c_0^2$, c_0 is the first order value of c) yields to the first order expressions

$$q_s = \left(\vec{u} + \frac{1}{\rho_0 c_0^2} p\vec{U}_0 \right) \cdot \vec{e}_n \tag{30}$$

$$\vec{f}_s = \left(p + \rho_0 \vec{U}_0 \cdot \vec{u} \right) \vec{e}_n \,. \tag{31}$$

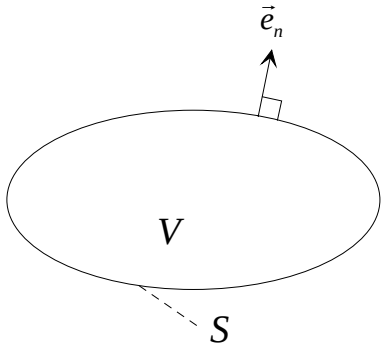

Figure 1. Scattering object with volume V and surface S.

If the Huygens' surface is a true rigid surface, the normal and tangential velocity disappears on the surface. In that case the Huygens' monopole distribution vanishes and the dipole distribution is in the general case

$$\vec{f}_s = \left[p + \rho\left(\vec{U}_0 \cdot \vec{u} + \tfrac{1}{2} \vec{u} \cdot \vec{u} \right) \right] \vec{e}_n - \vec{e}_n \cdot \overline{\overline{\sigma'}}, \tag{32}$$

and in the linearized case with small losses similar to Equation (31).

So, the effects of a scattering or absorbing surface on any sound field can be obtained by integrating the fields of the Huygens' monopole and dipole distributions at the surface, which distributions can be obtained from the actual fields at the surface using Equations (28) and (29) in the general case, Equations (30) and (31) in the linearized case with small losses, and Equation (32) in the case of a rigid reflecting surface, the last case reducing to Equation (31) in the linearized case with small losses.

The vortices act as quadrupole sources, as stated in the previous section. Because the effect of the static and solenoidal perturbation velocity on the reflection of sound from solid boundaries is mainly of dipole type (and also of monopole type if the boundary is not infinitely rigid), and the sound radiation of a dipole distribution is typically stronger than that of a quadrupole distribution, it can be deduced that the turbulent flow may cause the scattered sound to be even stronger than the original sound of the turbulences. This is the case when the solenoidal turbulent perturbation velocity at the boundary is high, imparting high fluctuating forces to the boundary [1], in which case the turbulences, besides acting directly as aerodynamic sound sources, are coupled to sound through the boundary.

5. Noise of high-Reynolds'-number subsonic cold-air jet

Suppose a laminar unrotational flow with a high Reynolds' number and velocity amplitude U_j comes out from a convergent nozzle, see Figure 2. An annular mixing layer forms between the flow and the surrounding fluid, beginning from the edge of the nozzle. Within a distance of $D/2$ from the nozzle, where D is the diameter of the nozzle, the velocity transforms into solenoidal and especially into solenoidal static and perturbation velocity (turbulence) in the mixing layer. The mixing layer spreads linearly, and at a distance of $4D$ it fills the whole jet. At the beginning of the inside of the mixing layer, there remains a region called a potential core where the static velocity remains unrotational and laminar. The longitudinal correlation length l of the vortices of the solenoidal perturbation velocity is about $l = 0.1\ r$, where r is the distance from the nozzle, whereas the transversal correlation length is half of that. In the fully developed region, the correlation length is independent of the distance, up to distance 20 D. The correlation of an eddy falls exponentially with time, the time constant being $\tau = 5l/U_j$ at the centerline of the mixing region. The eddy convection velocity U_c in the center of the mixing layer is equal to the static velocity U_0, being about $U_c = U_0 = 0.62\ U_j$. In the transition region the solenoidal perturbation velocity begins to fall with distance from the nozzle, and in the fully developed region it falls as $1/r^2$ to the right. [1]

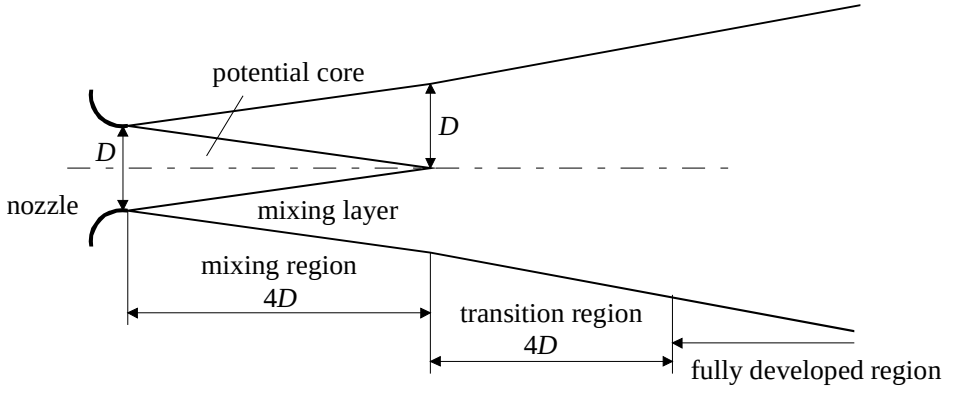

Figure 2. Jet structure [1].

The profile of the solenoidal perturbation velocity in the mixing layer is presented in Figure 3. It can be seen that the maximum ($\approx 0.16\ U_j$) is on the centerline of the mixing layer and falls near zero at the surfaces of the mixing layer [1].

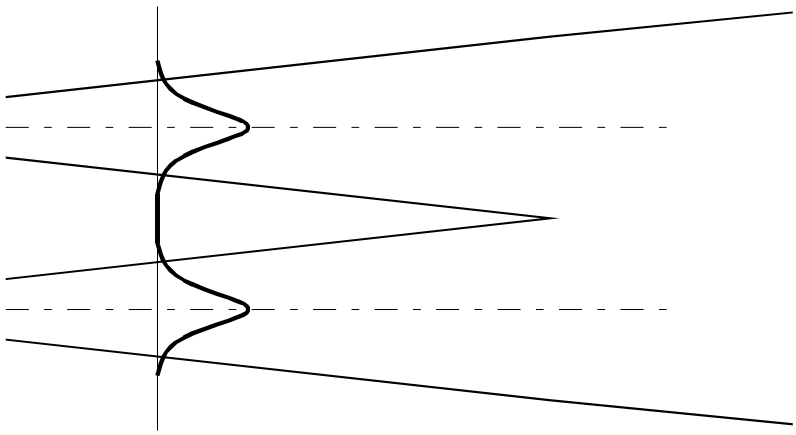

Figure 3. The profile of the solenoidal perturbation velocity in the mixing layer [1].

The profile of the static velocity in the mixing layer is presented in Figure 4. Because the irrotational part of the static velocity is constant across the jet, the solenoidal static velocity causes the total static velocity to fall gradually to zero at the outer surface of the jet.

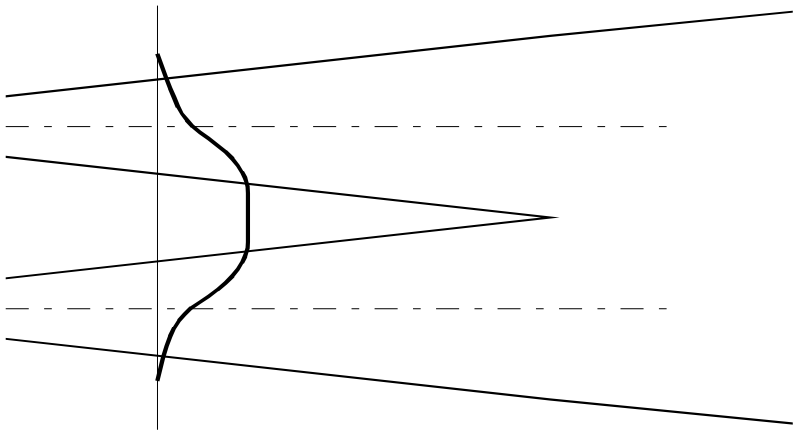

Figure 4. The profile of the static velocity in the mixing layer [1].

Because, generally, wavelength λ is the wave speed divided by frequency f, the wavelength of the eddy convection is $\lambda = U_c/f$ and the wavelength of the sound generated by the turbulences is $\lambda = c_0/f$.

The sound power per unit length P' generated by the mixing layer is independent of distance, being

$$P' = 6.5 \cdot 10^{-7} K \frac{\rho_0 U_j^8 D}{c_0^5} \frac{1 + M_c^2}{\left(1 - M_c^2\right)^4}, \tag{33}$$

where K is a constant near one, depending on the configuration, and $M_c = U_c/c_0$ is the convection Mach number. The numerical factor being so small is a consequence of the inefficiency of the quadrupole type sources. The power per unit length is presented in Figure 5 as a function of distance from the nozzle. It can be seen that most of the sound power originates from the mixing region, especially at high frequencies, some of it from the transition region, and the fully developed region has less effect on the sound power. [1]

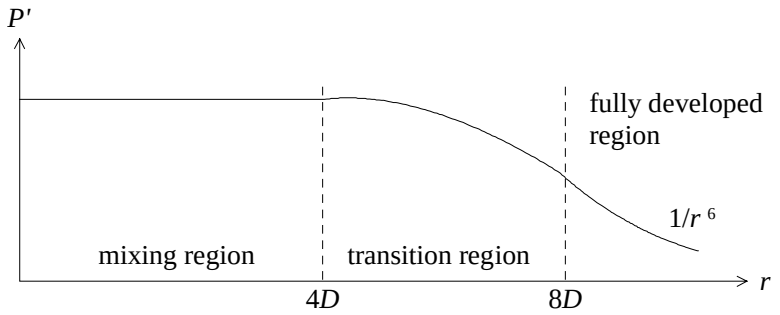

Figure 5. Power per unit length [1].

The spectrum of the jet noise is of broadband character, having its maximum at the Strouhal number being one [1], see Figure 6. The Strouhal number S is defined as

$$S = \frac{fD}{U_j}\left(1 - M_c \cos\theta\right), \tag{34}$$

where θ is the angle between the observation direction and the jet axis. The Doppler effect is included in the Strouhal number. Because of the Doppler effect, the observer downstream hears higher peak frequency, and the observer upstream hears lower peak frequency than the observer beside the jet [1].

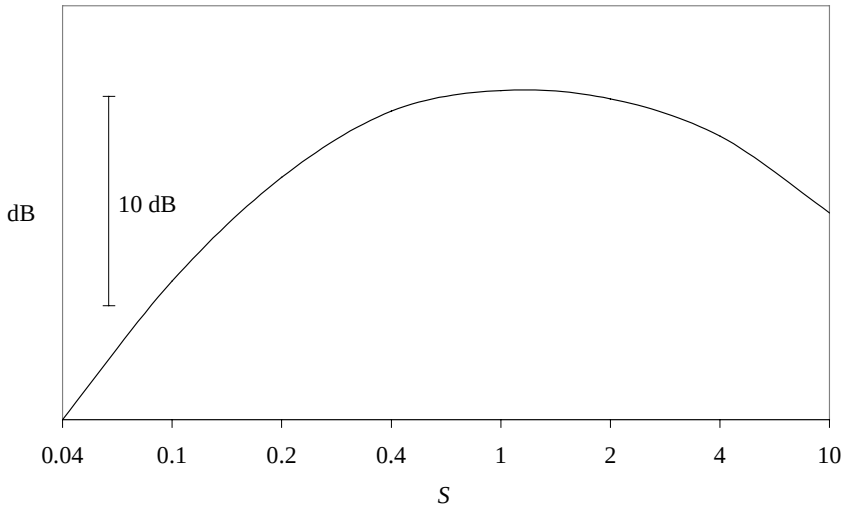

Figure 6. One-third octave spectrum of the jet noise as a function of the Strouhal number S [1].

The radiation pattern of the sound radiation is approximately proportional to $(1 - M_c \cos\theta)^{-5}$ [1]. The pattern is presented in Figure 7 for three convection Mach numbers. Other radiation patterns are also presented in [1], based on different theories. In each case, the typical radiation pattern of a quadrupole distribution is totally masked by convectional effects of the flow, which arise from the motion of the turbulent eddies relative to the observer.

According to Snell's law, the sound propagating in the jet in the jet flow direction will be refracted sidewards. Because of this, especially at high frequencies, a local aerodynamic source point in the jet at a radial distance of r_0 from the jet axis with sound speed $c(r_0)$ and jet Mach number $M(r_0)$ (local flow velocity of the jet divided by the ambient speed of sound c_0) does not radiate sound into a cone $\theta < \theta_c$ around the jet axis, where $\theta_c = \arccos\{1/[M(r_0) + c(r_0)/c_0]\}$. This leads to a cone existing in the center of the downstream jet axis, wherein the far field sound is greatly reduced ("zone of silence"). The depth of

the zone of silence increases with increasing frequency. The refraction tends to decline the lobe of the maximum radiation at small angles (< 20°) with respect to the jet axis. [1]

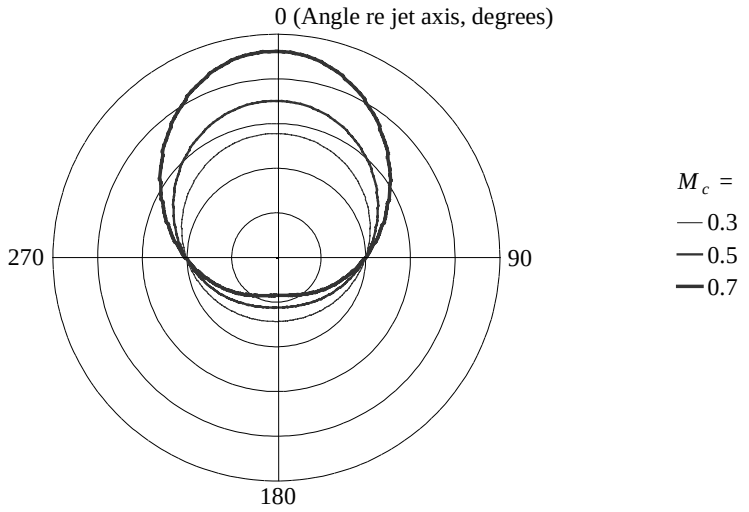

Figure 7. Radiation pattern of the jet noise at three convection Mach numbers. The difference between the circles is 10 dB. The decline of the radiation pattern due to the refraction caused by the flow is not taken into account.

6. Turbulent boundary layer as a noise source

When a flow U_{01} attacks a plate parallel to its surface, see Figure 8, the tangential velocity must be zero just on the surface, due to viscous drag of the fluid. Consider that the incoming flow is laminar and unrotational. At the surface there arises a laminar solenoidal tangential velocity U_{02}, decaying exponentially from the surface. The sum U_0 of the new velocity component and the original flow is zero on the surface, and at some distance from the surface the solenoidal velocity is small enough so that only the original unrotational velocity can be detected. The distance region where the solenoidal velocity affects is called the laminar boundary layer. The laminar boundary layer gets thicker as the flow passes along the surface. With Reynolds' numbers high enough, as the flow passes over some distance from the front edge of the plate, solenoidal perturbation velocity (unsteady vortices, turbulence) begins to form. These vortices obtain momentum from the fluid, and beyond a transition region they form a turbulent boundary layer growing with distance from the front edge of the plate. The boundary layer thickness δ obeys $\delta = 0.377x\,[\mu/(\rho U_{01}x)]^{1/5}$, where x is the distance from the edge of the plate [3]. The static velocity obeys in the boundary layer (not very close to the plate) $U_0 = U_{01}(y/\delta)^{1/7}$, where y is the perpendicular distance from the plate [3]. A viscous sublayer with a less solenoidal perturbation velocity is below the fully turbulent zone of the turbulent boundary layer, and a buffer zone connects them [4], see Figure 8. The viscous sublayer has been referred to as the laminar sublayer as well [3], but recent experimental and numerical investigations have shown that in fact this region is not laminar [4]. The different zones in the turbulent boundary layer extend to the following ranges from the plate surface [4]

$$\begin{aligned} 0 < y\frac{u_\tau}{\nu} < 2...8 &\Rightarrow \text{viscous sublayer} \\ 2...8 < y\frac{u_\tau}{\nu} < 2...50 &\Rightarrow \text{buffer zone} \\ 50 < y\frac{u_\tau}{\nu} &\Rightarrow \text{fully turbulent zone,} \end{aligned} \tag{35}$$

where ν is the kinematic viscosity $\nu = \mu / \rho_0$ and u_τ is the friction velocity $u_\tau = \sqrt{(\tau_\omega / \rho_0)} = U_{01}\sqrt{(c_f / 2)}$ (a characteristic velocity depending on the roughness of

the surface; the friction velocity is higher with rougher surfaces, τ_ω is the shear stress at the plate surface, c_f is the skin-friction coefficient). The solenoidal velocity (and thus the turbulent perturbation velocity) near the boundary is proportional to the friction velocity [2]. The majority of the turbulence energy is produced in the viscous sublayer and the buffer zone [4]. Most of the energy in a turbulent flow is contained in large eddies and the lifespan of the large-scale fluctuations is relatively long. The energy associated with smaller eddies is smaller and their life span is considerably shorter [4].

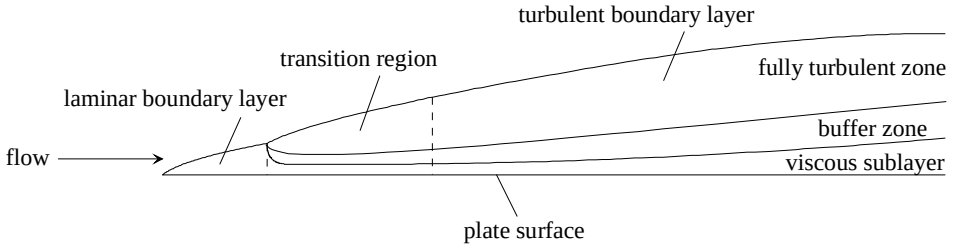

Figure 8. Flow generating a turbulent boundary layer on a plate [3, 4].

The arising velocity components act as aerodynamic sound sources according to Section 2.

A typical form of the autospectrum in the wavenumber domain of the flow noise at a plane, rigid surface is shown in Figure 9. The quantity k_1 is the wavenumber component in the x-direction, the quantity k_2 is the orthogonal wavenumber component at the plane, and $\vec{k}$ is the vector having k_1 and k_2 as components at the plane. The spectrum has two maxima: one at $k_1 = \omega/U_c$ with k_2 small (convective peak) and another at the acoustic wavenumber with an absolute value of ω/c_0 (sonic peak), where ω is the angular frequency $\omega = 2\pi f$. At lower wavenumbers ($k_1 < \omega/c_0$, supersonic region) the waves have a high supersonic surface phase speed ($> c_0$) and the wavenumber spectrum is constant. At higher wavenumbers ($k_1 > \omega/c_0$, subsonic region) the waves have a low subsonic surface phase speed ($< c_0$). The sonic and supersonic spectral components at the surface generate active propagating sound, and the subsonic spectral components generate mainly reactive, essentially incompressible near-field sound field. [2]

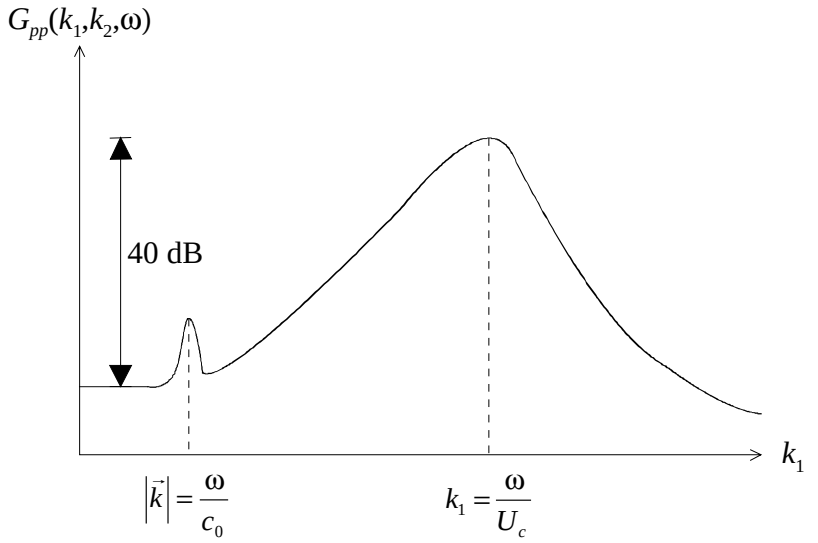

Figure 9. Autospectrum in the wavenumber domain of flow noise at a plane, rigid surface [2].

Because wavenumber k and wavelength λ have a relation $k = 2\pi / \lambda$, the wavelength at the convective peak is $\lambda = U_c / f$ and at the sonic peak it is $\lambda = c_0 / f$.

According to the Corcos' model [7], the spatial autocorrelation function of the noise R_{pp} (inverse spatial Fourier transform of the autospectrum G_{pp}) can be expressed in the following separable form

$$R_{pp}(\xi,\omega) = \Phi(\omega) A\left(\frac{\omega\xi_1}{U_c}\right) B\left(\frac{\omega\xi_2}{U_c}\right) \mathrm{e}^{-\mathrm{j}\omega\xi_1/U_c}, \tag{36}$$

where ω is the angular frequency, ξ_1 and ξ_2 are the spatial variables of the autocorrelation function in the flow direction and in the direction orthogonal to the flow on the plane, Φ is the frequency dependent part of the formula, and A and B are the spatial parts of the formula and they are to be determined from experimental data. Within errors of second order, functions A and B can be approximated by exponentials [7]

$$\begin{aligned} A(x) &= \mathrm{e}^{-\alpha_1|x|} \\ B(x) &= \mathrm{e}^{-\alpha_2|x|}, \end{aligned} \tag{37}$$

where α_1 and α_2 are to be determined from experimental data. Typical values for α_1 are between 0.11 and 0.12, and for α_2 between 0.7 and 1.2 [8].

The autospectrum can be obtained by the spatial Fourier transform of the autocorrelation function to yield [2]

$$G_{pp}(k_1, k_2, \omega) = \left(\frac{U_c}{\omega}\right)^2 \Phi(\omega) \hat{A}\left(\frac{k_1 U_c}{\omega} - 1\right) \hat{B}\left(\frac{k_2 U_c}{\omega}\right), \tag{38}$$

where $\hat{A}$ and $\hat{B}$ are the Fourier transforms of *A* and *B*. If functions *A* and *B* are approximated by the exponentials in Equation (37), the autospectrum in the Corcos' model can be presented as

$$G_{pp}(k_1, k_2, \omega) = \left(\frac{2U_c}{\omega}\right)^2 \Phi(\omega) \frac{\alpha_1}{\alpha_1^2 + \left(\frac{k_1 U_c}{\omega} - 1\right)^2} \frac{\alpha_2}{\alpha_2^2 + \left(\frac{k_2 U_c}{\omega}\right)^2}. \tag{39}$$

It can be clearly seen that, according to the Corcos' model, there is a maximum in the autospectrum at $k_1 = \omega/U_c$. The Corcos' model works well near the convective peak but overpredicts the autospectrum at low sonic and supersonic wavenumbers [2].

In the Efimtsov's model [9], the correlation lengths $l_1 = U_c / (\alpha_1 \omega)$ and $l_2 = U_c / (\alpha_2 \omega)$ of the Corcos' model are replaced by

$$\begin{aligned}
l_1 &= \delta \sqrt{\left(\frac{a_1 Sh}{U_c / u_\tau}\right)^2 + \frac{a_2^2}{Sh^2 + (a_2 / a_3)^2}} \\
l_2 &= \begin{cases} \delta \sqrt{\left(\frac{a_4 Sh}{U_c / u_\tau}\right)^2 + \frac{a_5^2}{Sh^2 + (a_5 / a_6)^2}}, & M_0 \le 0.75 \\ \delta \sqrt{\left(\frac{a_4 Sh}{U_c / u_\tau}\right)^2 + a_7^2}, & M_0 \ge 0.9 \end{cases} \\
Sh &= \frac{\omega \delta}{u_\tau} \\
a_1 &= 0.1,\ a_2 = 72.8,\ a_3 = 1.54,\ a_4 = 0.77,\ a_5 = 548,\ a_6 = 13.5,\ a_7 = 5.66,
\end{aligned} \tag{40}$$

to take into account the dependence of the spatial correlation on the boundary layer thickness and the spatial separation. Term $M_0 = U_{01} / c_0$ is the free-stream Mach number.

In the Smol'yakov's and Tkachenko's model [10], the dependence of the spatial correlation on the boundary layer thickness and the spatial separation is taken into account but with a combined correlation rather than with the pure lateral and longitudinal correlations. Their expression for the autospectrum is

$$G_{pp}(k_1,k_2,\omega) = \frac{2\pi}{m_0}\left(\frac{U_c}{\omega}\right)^2 \Phi(\omega)A(\omega)h(\omega)\left[F(k_1,k_2,\omega) - \Delta F(k_1,k_2,\omega)\right]$$

$$A(\omega) = \alpha_1\sqrt{1 - \frac{\mu_1 U_c}{\alpha_1\omega\delta^*} + \left(\frac{\mu_1 U_c}{\alpha_1\omega\delta^*}\right)^2}$$

$$h(\omega) = \left[1 - \frac{m_1 A(\omega)}{m_0 n^2\sqrt{1 + A^2(\omega) - m_1 n}}\right]^{-1}$$

$$F(k_1,k_2\omega) = \left[A^2(\omega) + \left(\frac{k_1 U_c}{\omega} - 1\right)^2 + \left(\frac{k_2 U_c}{m_0\omega}\right)^2\right]^{-3/2} \qquad (41)$$

$$\Delta F(k_1,k_2,\omega) = \frac{1}{n}\left\{1 + A^2(\omega) + \frac{n}{m_1}\left[\left(\frac{k_1 U_c}{\omega} - m_1\right)^2 + \left(\frac{k_2 U_c}{\omega}\right)^2 - m_1^2\right]\right\}^{-3/2}$$

$$m_1 = \frac{1 + A^2(\omega)}{5n - 4 + A^2(\omega)}$$

$$m_0 = 6.45,\ \alpha_1 = 0.124,\ \mu_1 = 0.031,\ n = 1.005,$$

where δ^* is the boundary layer displacement thickness $\delta^* = \delta/8$.

In [11] Ffowcs Williams derived an expression for the autospectrum $G_{pp}(k_1,k_2,\omega)$ containing several unknown constants and functions to be determined experimentally. Based on that, Hwang and Geib [12] proposed a simplified version in which the autospectrum of the Corcos' model is simply multiplied by $(U_c|k|/\omega)$. At low sonic and supersonic wavenumbers, this corrected model is more suitable than the Corcos' model.

The autospectrum is, according to the Chase's first formula [13],

$$G_{pp}(k_1,k_2,\omega)=(2\pi)^3\rho^2u_\tau^3\left[\frac{C_Mk_1^2}{\left(K_+^2+(b_M\delta)^{-2}\right)^{5/2}}+\frac{C_T\left|\vec{k}\right|^2}{\left(K_+^2+(b_T\delta)^{-2}\right)^{5/2}}\right]$$

$$K_+^2=\left(\frac{\omega-U_ck_1}{hu_\tau}\right)^2+\left|\vec{k}\right|^2 \qquad (42)$$

$$C_M=0.0745,\ C_T=0.0475,\ b_M=0.756,\ b_T=0.378,\ h=3.$$

The Chase's first formula does not work in the supersonic region [5]. The Chase's second formula [14], working better at low sonic and supersonic wavenumbers, is

$$G_{pp}(k_1,k_2,\omega)=(2\pi)^3\frac{\rho^2u_\tau^3}{\left[K_+^2+(b\delta)^{-2}\right]^{5/2}}\left[C_Mk_1^2+C_T\left|\vec{k}\right|^2\frac{K_+^2+(b\delta)^{-2}}{\left|\vec{k}\right|^2+(b\delta)^{-2}}\right]$$

$$K_+^2=\left(\frac{\omega-U_ck_1}{hu_\tau}\right)^2+\left|\vec{k}\right|^2 \qquad (43)$$

$$hC_M=0.466,\ hC_T=0.014,\ b=0.75,\ h=3.$$

The Chase's second formula works well within a range consisting of subsonic and supersonic regions [5].

Sevik's experimental model gives for the autospectrum in the highly supersonic region [2]

$$G_{pp}(0,0,\omega)=5.6\frac{\rho^2u_\tau^4\delta^{*3}M_0^2}{U_{01}}\left(\frac{\omega\delta^*}{U_{01}}\right)^{-4.5}. \qquad (44)$$

It can be noticed that with a typical value $\omega\delta^*/U_{01}=3$ the level at the convective peak exceeds that at low wavenumbers by 40 dB [2]. The autospectrum is proportional to the fourth power of the friction velocity, so the sound due to turbulences is highly dependent on the roughness of the surface.

In some expressions of the autospectrum, there are differences compared with the expressions of the references, containing powers of 2π. This is due to the different definitions of the autospectrum integral.

The autospectrum near the sonic condition ($|k| = \omega / c_0$) depends on the geometry or aerodynamic source size, most of the energy arriving at grazing incidence from the upstream direction [2].

There can exist downstream propagating wavenumber components near the sonic peak having subsonic surface phase speed in the boundary layer and supersonic outside it (the static velocity is superimposed to the phase speed). This kind of a speed profile makes the waves to refract towards the surface, so the waves remain trapped near the surface like with a two-dimensional waveguide. Thus the perturbation fields will only decay with the inverse square root of the distance while propagating near the surface. The situation is vice versa with the upstream propagating wavenumber components near the sonic peak: the waves tend to refract outwards from the surface and decay more rapidly. This effect enhances the sonic peak in the downstream radiation and may eliminate it in the upstream radiation. [2]

The convective peak in the autospectrum in the wavenumber domain is the main origin of the sound power transmitted through and radiated by the plate surface itself [5]. The vibration of the plate, causing the sound transmission and radiation, is mainly resonant and composed of wavenumbers the components of which in the convection direction are near the convective peak (hydrodynamic coincidence). This causes the frequency spectrum of the transmitted and radiated sound to lie below the hydrodynamic coincidence frequency $f \leq f_{crM} = M_c^2 f_{cr}$, where f_{cr} is the critical frequency of the plate [5, 15]. With subsonic convection velocities, this frequency range is below the critical frequency of the plate. The situation is similar when a turbulent jet impinges on a surface if the convective Mach number is replaced by the corresponding Mach number component along the plate surface $M_c / |\cos\alpha|$, where α is the propagation angle of the convection with respect to the plate surface.

Because the major part of the propagating sound is due to the sonic and supersonic parts of the wavenumber spectrum, it may be advisable to use the Chase's second formula, which, with suitably chosen constants, works well

within a range consisting of subsonic and supersonic regions [2, 5]. However, because the convective peak in the autospectrum in the wavenumber domain is the main origin of the sound power transmitted through and radiated by the plate surface itself, the detailed shape of the convective peak is important in the model used in connection with the sound transmission and radiation of the plate. The inability of the Corcos' model to account for the dependence of the correlation length on the boundary layer thickness rules it out as a candidate [5]. According to Graham [5], the Smol'yakov's and Tkachenko's model would be a good choice in that case.

7. Summary

The aerodynamic sound source of a turbulent flow has been defined based on two assumptions:

- the terms presenting the viscous and thermal losses in the Navier-Stokes' equation are not considered as source terms

- the aerodynamic sound source quantities can be (approximately) separated from the acoustic field variables.

This leads to a solution where the aerodynamic source is composed of the Reynolds' stress, all the terms containing irrotational perturbation velocity and perturbation density excluded. All the terms in the aerodynamic source part of the Reynolds' stress contain the solenoidal perturbation velocity, i.e. vortices, as an element. Some source terms contain the solenoidal perturbation velocity as a second-order element. The other relevant terms contain both the solenoidal perturbation velocity and the static velocity as elements. The perturbation–perturbation solenoidal velocity interaction is called self-noise while the perturbation–static velocity interaction is called shear-noise. The perturbation–static velocity interaction can be seen as a phenomenon where the perturbation vorticity is carried along with the static flow. The vortices act as quadrupole sources.

Because the Reynolds' stress behaves like a momentum source distribution, its physical significance is that it gives momentum to the acoustic field from the static flow. The Reynolds' stress can be a remarkable source of sound only in the case of a high Reynolds' number, in which case the vortices appear turbulent.

The equivalent Huygens' sources have been defined with the flow present. The effects of a scattering or absorbing surface on any sound field can be obtained by integrating the fields of the Huygens' monopole and dipole distributions at the surface. Because the effect of the static and turbulent velocity on the reflection of sound from solid boundaries is mainly of dipole type (and also of monopole type if the boundary is not infinitely rigid), and the sound radiation of a dipole distribution is typically stronger than that of a quadrupole distribution, the turbulent flow may cause the scattered sound to be even stronger than the original sound of the turbulences. This is the case when the solenoidal turbulent

perturbation velocity at the boundary is high, imparting high fluctuating forces to the boundary, in which case the turbulences, besides acting directly as aerodynamic sound sources, are coupled to sound through the boundary.

The generation and properties of the noise of a high-Reynolds'-number subsonic cold-air jet has been studied. The jet structure, beginning from a nozzle and developing gradually to solenoidal and turbulent, consists of an annular mixing region with a potential core having laminar flow inside, a transition region, and a fully developed region. Most of the sound power originates from the mixing region, especially at high frequencies, some of it from the transition region, and the fully developed region has less effect on the sound power.

The spectrum of the jet noise is of broadband character, having its maximum at the Strouhal number being one. Because of the Doppler effect, the observer downstream hears higher peak frequency, and the observer upstream hears lower peak frequency than the observer beside the jet.

The typical radiation pattern of a quadrupole distribution is totally masked by convectional effects of the jet flow, which arise from the motion of the turbulent eddies relative to the observer. The convectional effects tend to generate a radiation pattern where the sound is greatly enhanced in the flow direction. According to Snell's law, the sound propagating in the jet in the jet flow direction will be refracted sidewards. This causes a cone centered on the downstream jet axis, wherein the far field sound is greatly reduced ("zone of silence"). The depth of the zone of silence increases with increasing frequency. The refraction tends to decline the lobe of the maximum radiation at small angles with respect to the jet axis.

When a flow attacks a plate parallel to its surface, there arises a laminar solenoidal tangential velocity, decaying exponentially from the surface. The sum of the new velocity component and the original flow is zero on the surface and at a distance from the surface, called the laminar boundary layer thickness, the solenoidal velocity is small enough so that only the original velocity can be detected. The laminar boundary layer gets thicker as the flow passes along the surface. With Reynolds' numbers high enough, as the flow passes over some distance from the front edge of the plate, solenoidal perturbation velocity (unsteady vortices, turbulence) begins to form. Beyond a transition region, these

vortices form a turbulent boundary layer growing with distance from the front edge of the plate. A viscous sublayer with a less solenoidal perturbation velocity is below the fully turbulent zone of the turbulent boundary layer, and a buffer zone connects them. The majority of the turbulence energy is produced in the viscous sublayer and the buffer zone. Most of the energy in a turbulent flow is contained in large eddies rather than in smaller ones, and the lifespan of the large eddies is longer than that of the small ones. The arising velocity components act as aerodynamic sound sources.

The wavenumber spectrum in the turbulent boundary layer has two maxima: the convective peak at a high (subsonic) wavenumber and the sonic peak at the acoustic wavenumber. At lower (supersonic) wavenumbers the wavenumber spectrum is constant. The autospectrum is highly dependent on the roughness of the surface. The sonic and supersonic spectral components at the surface generate active propagating sound, and the subsonic spectral components generate mainly reactive, essentially incompressible near-field sound field. With the spectral components near the sonic condition, most of the acoustic energy arrives at field points at grazing incidence from the upstream direction.

The Corcos' model for the spatial autocorrelation and the autospectrum of the sound, due to the turbulent boundary layer, is based on the separation of the lateral and longitudinal effects. It works well near the convective peak but overpredicts the autospectrum at sonic and supersonic wavenumbers. In the Emfitsov's model and in the Smol'yakov's and Tkachenko's model, the dependence of the spatial correlation on the boundary layer thickness and the spatial separation is taken into account. The Ffowcs Williams' model, simplified by Hwang and Geib, is more suitable at sonic and supersonic wavenumbers than the Corcos' model. The Chase's second formula works well within a range consisting of subsonic and supersonic regions. Sevik's model works well in the highly supersonic region.

There can exist downstream propagating wavenumber components near the sonic peak having subsonic surface phase speed in the boundary layer and supersonic outside it (the static velocity is superimposed to the phase speed). This makes the waves refract towards the surface, so the waves remain trapped near the surface as with a two-dimensional waveguide. The situation is vice versa with the upstream propagating wavenumber components: the waves tend

to refract outwards from the surface. This effect enhances the sonic peak in the downstream radiation and may eliminate it in the upstream radiation.

The convective peak in the autospectrum in the wavenumber domain is the main origin of the sound power transmitted through and radiated by the plate surface itself. The vibration of the plate, causing the sound transmission and radiation, is mainly resonant and composed of wavenumbers the components of which in the convection direction are near the convective peak (hydrodynamic coincidence). This causes the frequency spectrum of the transmitted and radiated sound to lie below the hydrodynamic coincidence frequency. The situation is similar when a turbulent jet impinges on a surface if the convective Mach number is replaced by the corresponding Mach number component along the plate surface.

Because the major part of the propagating sound is due to the sonic and supersonic parts of the wavenumber spectrum, it may be advisable to use the Chase's second formula, which, with suitably chosen constants, works well within a range consisting of subsonic and supersonic regions. However, because the convective peak in the autospectrum in the wavenumber domain is the main origin of the sound power transmitted through and radiated by the plate surface itself, the detailed shape of the convective peak is important in the model used in connection with the sound transmission and radiation of the plate. The Smol'yakov's and Tkachenko's model would be a good choice in that case.

References

1. Goldstein, M. E. Aeroacoustics. 1st ed. New York: McGraw-Hill. 1976. 293 p. ISBN 0-07-023685-2

2. Crighton, D. G., Dowling, A. P., Williams, J. E. F., Heckl, M., Leppington, F. G. Modern methods in analytical acoustics. 1st ed. London: Springer-Verlag. 1992. 738 p. ISBN 3-540-19737-0

3. Daugherty, R. L., Franzini, J. B., Finnemore, E. J. Fluid mechanics with engineering applications. 8th ed. New York, USA: McGraw-Hill Book Company. 1985. 599 p. ISBN 0-07-015441-4

4. Hoffmann, K. A., Chiang, S. T. Computational fluid dynamics, Volume III. 4th ed. Wichita, Kansas, USA: Engineering Education Systems. 2000. 175 p. ISBN 0-9623731-6-8

5. Graham, W. R. A comparison of models for the wavenumber-frequency spectrum of turbulent boundary layer pressures. J. Sound Vib. 1997. Vol. 206, no. 4, pp. 541–565.

6. Pierce, A. D. Acoustics. An introduction to its physical principles and applications. 2nd ed. New York, USA: Acoustical Society of America. 1991. 653 p. ISBN 0-88318-612-8

7. Corcos, G. M. Resolution of pressure in turbulence. J. Acoust. Soc. Am. 1963. Vol. 35, no. 2, pp. 192–199.

8. Hwang, Y. F., Maidanik, G. A wavenumber analysis of the coupling of a structural mode and flow turbulence. J. Sound Vib. 1990. Vol. 142, no. 1, pp. 135–152.

9. Efimtsov, B. M. Characteristics of the field of turbulent wall pressure fluctuations at large Reynolds numbers. Sov. Phys. Acoust. 1982. Vol. 28, no. 4, pp. 289–292.

10. Smol'yakov, A. V., Tkachenko, V. M. Model of a field of pseudosonic turbulent wall pressures and experimental data. Sov. Phys. Acoust. 1992. Vol. 37, no. 6, pp. 627–631.

11. Ffowcs Williams, J. E. Boundary-layer pressures and the Corcos model: a development to incorporate low-wavenumber constraints. J. Fluid Mech. 1982. Vol. 125, pp. 9–25.

12. Hwang, Y. F., Geib, F. E. Estimation of the wavevector–frequency spectrum of turbulent boundary layer wall pressure by multiple linear regression. J. Vib. Ac. Stress and Rel. in Design. 1984. Vol. 106, pp. 334–342.

13. Chase, D. M. Modeling the wavevector–frequency spectrum of turbulent boundary layer wall pressure. J. Sound Vib. 1980. Vol. 70, no. 1, pp. 29–67.

14. Chase, D. M. The character of the turbulent wall pressure spectrum at subconvective wavenumbers and a suggested comprehensive model. J. Sound Vib. 1987. Vol. 112, no. 1, pp. 125–147.

15. Totaro, N., Guyader, J.-L. Model of frequency averaged injected power into a plate excited by a turbulent boundary layer. Acta Acustica united with Acustica. 2003. Vol. 89, no. 4, pp. 647–657.

Published by

Vuorimiehentie 5, P.O.Box 2000, FIN–02044 VTT, Finland
Phone internat. +358 9 4561
Fax +358 9 456 4374

Series title, number and report code of publication

VTT Publications 513
VTT–PUBS–513

Author(s)
Uosukainen, Seppo

Title

Turbulences as sound sources

Abstract

The aerodynamic sound source of a turbulent flow with a high Reynolds' number is composed of two types of Reynolds' stress components containing turbulent vortices as elements: perturbation–perturbation solenoidal velocity interaction (self-noise) and perturbation–static velocity interaction (shear-noise). The vortices act as quadrupole sources. Near a scattering surface, a high turbulent velocity imparts high fluctuating forces to it and couples to sound causing the scattered sound to be even stronger than the original one. The high-Reynolds'-number subsonic cold-air jet structure, beginning from a nozzle and developing gradually to solenoidal and turbulent, consists of a mixing region, a transition region, and a fully developed region. Most of the sound power originates from the mixing region. The spectrum of the jet noise is of broadband character. The typical radiation pattern of a quadrupole distribution is totally masked by convectional effects of the jet flow, which tend to enhance the sound greatly in the flow direction. The sound propagating in the jet flow direction will be refracted sidewards, causing a cone centered on the downstream jet axis wherein the far field sound is greatly reduced (zone of silence), and tending to decline the lobe of the radiation pattern. When a flow attacks a plate parallel to its surface at Reynolds' numbers high enough, there begins to form unsteady vortices, forming a turbulent boundary layer. The wavenumber spectrum in the turbulent boundary layer has two maxima: the convective peak at a high subsonic wavenumber and the sonic peak at the acoustic wavenumber. The sonic and supersonic spectral components at the surface generate active propagating sound, most of the acoustic energy propagating at grazing incidence downstream. Downstream propagating sound due to the wavenumber components near the sonic peak refracts towards the surface, and upstream propagating sound refracts outwards from the surface, enhancing the sonic peak in the downstream radiation and possibly eliminating it in the upstream radiation. The convective peak at the surface leads to the hydrodynamic coincidence, causing sound transmission and radiation at frequencies below the hydrodynamic coincidence frequency.

Keywords
noise, jet noise, turbulence, turbulent flow, vortex flow, air jets, Reynolds' stress, boundary layers

Activity unit
VTT Building and Transport, Lämpömiehenkuja 3, P.O.Box 1804, FIN–02044 VTT, Finland

ISBN
951–38–6257–7 (soft back ed.)
951–38–6258–5 (URL:http://www.vtt.fi/inf/pdf/)

Project number
R2SU00573

Date	Language	Pages	Price
December 2003	English	42 p.	A

Name of project
FACE

Commissioned by
EU

Series title and ISSN
VTT Publications
1235–0621 (soft back ed.)
1455–0849 (URL: http://www.vtt.fi/inf/pdf/)

Sold by
VTT Information Service
P.O.Box 2000, FIN–02044 VTT, Finland
Phone internat. +358 9 456 4404
Fax +358 9 456 4374

VTT PUBLICATIONS

492 Himanen, Mervi. The Intelligence of Intelligent Buildings. The Feasibility of the Intelligent Building Consept in Office Buildings. 2003. 497 p.

493 Rantamäki, Karin. Particle-in-Cell Simulations of the Near-Field of a Lower Hybrid Grill. 2003. 74 p. + app. 61 p.

494 Heiniö, Raija-Liisa. Influence of processing on the flavour formation of oat and rye. 2003. 72 p. + app. 48 p.

495 Räsänen, Erkki. Modelling ion exchange and flow in pulp suspensions. 2003. 62 p. + app. 110 p.

496 Nuutinen, Maaria, Reiman, Teemu & Oedewald, Pia. Osaamisen hallinta ydinvoimalaitoksessa operaattoreiden sukupolvenvaihdostilanteessa. 2003. 82 s.

497 Kolari, Sirpa. Ilmanvaihtojärjestelmien puhdistuksen vaikutus toimistorakennusten sisäilman laatuun ja työntekijöiden työoloihin. 2003. 62 s. + liitt. 43 s.

498 Tammi, Kari. Active vibration control of rotor in desktop test environment. 2003. 82 p.

499 Kololuoma, Terho. Preparation of multifunctional coating materials and their applications. 62 p. + app. 33 p.

500 Karppinen, Sirpa. Dietary fibre components of rye bran and their fermentation *in vitro*. 96 p. + app. 52 p.

501 Marjamäki, Heikki. Siirtymäperusteisen elementtimenetelmäohjelmiston suunnittelu ja ohjelmointi. 2003. 102 s. + liitt. 2 s.

502 Bäckström, Mika. Multiaxial fatigue life assessment of welds based on nominal and hot spot stresses. 2003. 97 p. + app. 9 p.

503 Hostikka, Simo, Keski-Rahkonen, Olavi & Korhonen, Timo. Probabilistic Fire Simulator. Theory and User's Manual for Version 1.2. 2003. 72 p. + app. 1 p.

504 Torkkeli, Altti. Droplet microfluidics on a planar surface. 2003. 194 p. + app. 19 p.

505 Valkonen, Mari. Functional studies of the secretory pathway of filamentous fungi. The effect of unfolded protein response on protein production. 2003. 114 p. + app. 68 p.

506 Caj Södergård (ed.). Mobile television - technology and user experiences. Report on the Mobile-tv project. 2003. 238 p. + app. 35 p.

507 Rosqvist, Tony. On the use of expert judgement in the qualification of risk assessment. 2003. 48 p. + app. 82 p.

508 Parviainen, Päivi, Hulkko, Hanna, Kääriäinen, Jukka, Takalo, Juha & Tihinen, Maarit. Requirements engineering. Inventory of technologies. 2003. 106 p.

509 Sallinen, Mikko. Modelling and estimation of spatial relationships in sensor-based robot workcells. 2003. 218 p.

512 Kauppi, Tarja. Performance analysis at the software architectural level. 2003. 78 p.

513 Uosukainen, Seppo. Turbulences as sound sources. 2003. 42 p.

The sound source of a turbulent flow consists of two quadrupole-type Reynolds' stress components containing turbulent vortices: perturbation–perturbation and perturbation–static velocity interaction. The coupling of a high turbulent velocity to sound at a surface causes the scattered sound to be even stronger than the original one. The high-Reynolds'-number turbulent jet structure consists of a mixing region, a transition region and a fully developed region. Most of the sound originates from the first one. The convection of the jet flow enhances the sound in the flow direction but the refraction declines the main lobe. When a flow attacks a plate parallel to its surface at a high Reynolds' number, a turbulent boundary layer begins to form. Most of its sound propagates at grazing incidence downstream, and the refraction further emphasizes that.

Tätä julkaisua myy
VTT TIETOPALVELU
PL 2000
02044 VTT
Puh. (09) 456 4404
Faksi (09) 456 4374

Denna publikation säljs av
VTT INFORMATIONSTJÄNST
PB 2000
02044 VTT
Tel. (09) 456 4404
Fax (09) 456 4374

This publication is available from
VTT INFORMATION SERVICE
P.O.Box 2000
FIN–02044 VTT, Finland
Phone internat. +358 9 456 4404
Fax +358 9 456 4374

ISBN 951–38–6257–7 (soft back ed.)
ISSN 1235–0621 (soft back ed.)

ISBN 951–38–6258–5 (URL: http://www.vtt.fi/inf/pdf/)
ISSN 1455–0849 (URL: http://www.vtt.fi/inf/pdf/)

Seppo Uosukainen